Supplemental Information

Molecular and physical characteristics of aerosol at a remote marine free troposphere site: Implications for atmospheric aging

Simeon K. Schum[1], Bo Zhang[2,a], Katja Dzepina[1,b], Paulo Fialho[3], Claudio Mazzoleni[2,4] and Lynn R. Mazzoleni[1,2]

[1]Department of Chemistry, Michigan Technological University, Houghton, MI, USA
[2]Atmospheric Science Program, Michigan Technological University, Houghton, MI, USA
[3]Institute for Volcanology and Risk Assessment – IVAR, University of the Azores, Angra do Heroísmo, Portugal
[4]Department of Physics, Michigan Technological University, Houghton, MI, USA
[a]now at the National Institute of Aerospace, Hampton, VA, USA
[b]now at the Department of Biotechnology, University of Rijeka, Croatia

Correspondence to: Lynn R. Mazzoleni (lrmazzol@mtu.edu)

Table of Contents

Pico Mountain Observatory

Pico Mountain Observatory (PMO) is located in the summit caldera of Pico Mountain on Pico Island, in the Azores, Portugal (38.47 °N, 28.40 °W). The sampling site is located at an altitude of 2225 m asl. Pico mountain is the highest mountain in Portugal and in the central North Atlantic region (Honrath et al., 2008). The sampling site is often in the free troposphere as the marine boundary layer height in the area is normally between 500 and 2000 m (Kleissl et al., 2007; Rémillard et al., 2012; Zhang et al., 2017). At the site there is a variety of instrumentation such as a seven wavelength aethalometer, nephelometer, optical particle counter, and ozone detector. In various studies this site has been denoted as PMO, PICO-NARE, and OMP. Its identifying code is PIC in the NOAA database.

Supplemental Methods

Organic and Elemental Carbon Analysis

For each sample collected, a minimum of three circular 16 mm diameter filter punches were analyzed. If all three punches had consistent organic carbon concentrations (relative standard deviation, RSD < 15 %), the average value was used to determine the total loading of OC on the filter and in the air during the sampling period. If the replicates were inconsistent, more replicates were analyzed until at least three were consistent. Elemental carbon measurements were also obtained with this instrument, but in nearly all cases they were below the detection limit, so those values are not reported.

Ion Chromatography

PMO samples were also analyzed for major anions and cations using ion chromatography (IC). Anion analysis was performed using a Dionex ICS-2100 instrument (Thermo Scientific) with an AS-17-C analytical and guard column set (Thermo Scientific) using a KOH generator for gradient elution. The gradient elution had the following steps: -5 – 0 min., Equilibrate, 1 mM KOH, 0 – 15 min., Isocratic, 1 mM KOH, 15 – 20 min., Ramp, 1 – 10 mM KOH, 20 – 30 min., Isocratic, 10 mM KOH, 30 – 40 min., Ramp, 10 – 20 mM KOH, 40 – 45 min., Isocratic, 20 mM KOH, 45 – 55 min., and Ramp, 20 – 40 mM KOH. Cation analysis was performed using a Dionex ICS-1100 instrument with CS-12A analytical and guard column set (Thermo Scientific) and an isocratic 20 mM methanesulfonic acid eluent. The instruments were operated in parallel using split flow from autosampler. The samples were prepared using the California Air Resource Board method (California Environmental Protection Agency, 2011). Briefly, five square punches of 3.98 cm^2 each were taken from each filter and placed into a pre-cleaned 15 mL disposable centrifuge tube, to which 100 µL of isopropanol was added to help dissolve the less soluble organic species. Finally, 12 mL of 18.2 MOhm deionized water from an Easy Pure water system (Barnstead, ThermoFisher Waltham, MA, USA) were added to each centrifuge tube. These samples were then sonicated for 60 minutes with blue ice added to the sonication bath to keep the temperature below 25 ^{0}C. Once sonicated, the samples were stored in the refrigerator overnight and transferred with 0.45 um nylon syringe filters (Fisher Brand, Waltham, MA, USA) and sterile 3 mL syringes (BD, Franklin Lakes, NJ, USA) to 5 mL IC vials (Thermo Scientific, Waltham, MA, USA) the following day. The samples were then run on the IC system. After the ion concentrations were determined, they were background subtracted using field blanks from PMO.

Retroplume Analysis

Retroplume analysis was conducted using the Lagrangian particle dispersion model FLEXPART. (Seibert and Frank, 2004; Stohl et al., 2005; Owen and Honrath, 2009) The backward mode of FLEXPART was used to simulate backward transport trajectories from the PMO. The Global Forecast System (GFS) fields were used to drive FLEXPART. In the backward mode, hundreds of thousands of passive particles (tracer) were released from the receptor. The advection and dispersion of the particles were simulated backwards in time. The product of a backward simulation is an upwind spatial distribution of the particle residence times (average time an air parcel stays within a model grid cell), referred to as a "retroplume" (Seibert and Frank, 2004). In this study we report three specific events, one that took place on June 27 (19:00) -28 (19:00), 2013 (PMO-1), one on July 05 (15:00) - 06 (15:00), 2014 (PMO-2), and one on June 20 (15:00) - 21 (15:00), 2015 (PMO-3).

Supplemental Tables

Table S1. The ionization parameters for negative mode ESI FT-ICR MS for each of the samples are present in this table.

Sample	Spray Voltage (V)	Sheath Gas Flow (µL/min)	Source Temp (°C)
PMO-1 Rep 1	3.40	5.0	275
PMO-1 Rep 2	3.15	5.0	275
PMO-2 Rep 1	3.25	4.5	275
PMO-2 Rep 2	3.25	4.5	275
PMO-3 Rep 1	3.15	4.5	275
PMO-3 Rep 2	3.15	4.5	275

Table S2. Number of common species between this study and previous studies at PMO (Dzepina et al., 2015) and SPL (Mazzoleni et al., 2012). The percentages indicate the percent of common species for the sample indicated by the row names.

	PMO-1	PMO-2	PMO-3	Dzepina 2015	Mazzoleni 2012
PMO-1	X	1697 (53.6%)	1633 (51.5%)	2730 (86.2%)	1951 (61.6%)
PMO-2	1697 (80.0%)	X	1253 (59.1%)	1585 (74.7%)	1661 (78.3%)
PMO-3	1633 (89.7%)	1253 (68.8%)	X	1704 (90.6%)	1429 (76.0%)

Table S3. Molecular formula composition average values with standard error and number for each elemental group.

Sample	Group	O/C	H/C	DBE	OS_C	Number
PMO-1	CHO	0.46 ± 0.0074	1.28 ± 0.014	8.16 ± 0.130	-0.36± 0.023	1848
PMO-2	CHO	0.51 ± 0.0097	1.37 ± 0.015	6.59 ± 0.152	-0.36± 0.029	1281
PMO-3	CHO	0.45 ± 0.0075	1.36 ± 0.016	7.34 ± 0.178	-0.46± 0.026	1183
PMO-1	CHNO	0.48 ± 0.0070	1.21 ± 0.015	9.40 ± 0.180	-0.25± 0.020	1120
PMO-2	CHNO	0.58 ± 0.012	1.26 ± 0.015	8.03 ± 0.19	-0.10± 0.027	561
PMO-3	CHNO	0.48 ± 0.0077	1.24 ± 0.016	9.08 ± 0.185	-0.28± 0.069	608
PMO-1	CHOS	0.50± 0.019	1.77± 0.026	3.04± 0.218	-0.77± 0.056	200
PMO-2	CHOS	0.67± 0.0302	1.61± 0.029	3.89± 0.250	-0.27± 0.058	274
PMO-3	CHOS	0.41 ± 0.036	1.90 ± 0.078	1.72 ± 0.432	-1.1 ± 0.069	29

Table S4. Relative abundance weighted average values for the composition of molecular formulas in each molecular group.

Sample	Group	O/C_w	H/C_w	DBE_w	OSc_w
PMO-1	CHO	0.47 ± 0.14	1.31 ± 0.29	7.43 ± 3.68	-0.37 ± 0.44
PMO-2	CHO	0.55 ± 0.17	1.35 ± 0.25	6.43 ± 3.66	-0.26 ± 0.45
PMO-3	CHO	0.44 ± 0.14	1.37 ± 0.31	6.93 ± 3.82	-0.48 ± 0.48
PMO-1	CHNO	0.49 ± 0.15	1.2 ± 0.26	9.44 ± 3.09	-0.22 ± 0.32
PMO-2	CHNO	0.59 ± 0.14	1.25 ± 0.19	8.20 ± 2.19	-0.07 ± 0.31
PMO-3	CHNO	0.49 ± 0.14	1.23 ± 0.21	9.25 ± 2.41	-0.25 ± 0.27
PMO-1	CHOS	0.48 ± 0.14	1.78 ± 0.35	2.87 ± 3.28	-0.82 ± 0.53
PMO-2	CHOS	0.74 ± 0.34	1.57 ± 0.23	4.05 ± 2.45	-0.08 ± 0.70
PMO-3	CHOS	0.40 ± 14	1.90 ± 0.47	1.60 ± 4.29	-1.1 ± 0.68

Supplemental Figures

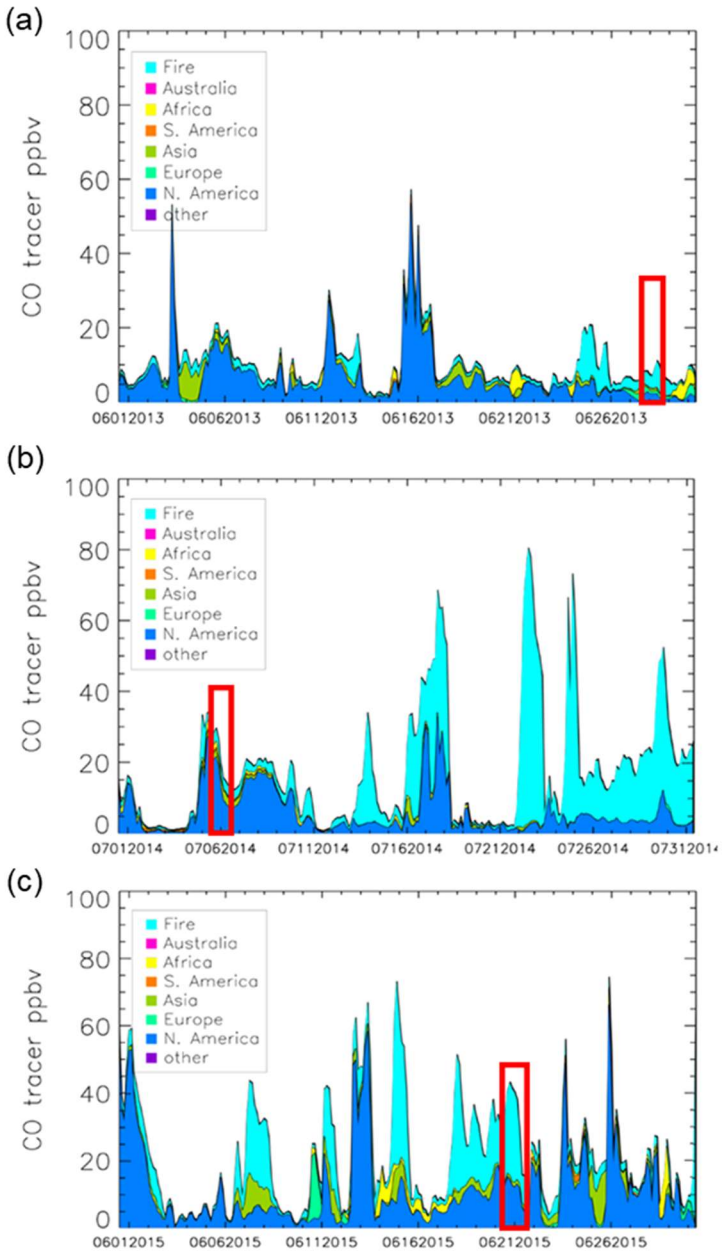

Figure S1. FLEXPART carbon monoxide source apportionment plot. PMO-1 (a), PMO-2 (b), PMO-3 (c). The red rectangle highlights the sampling period for each sample.

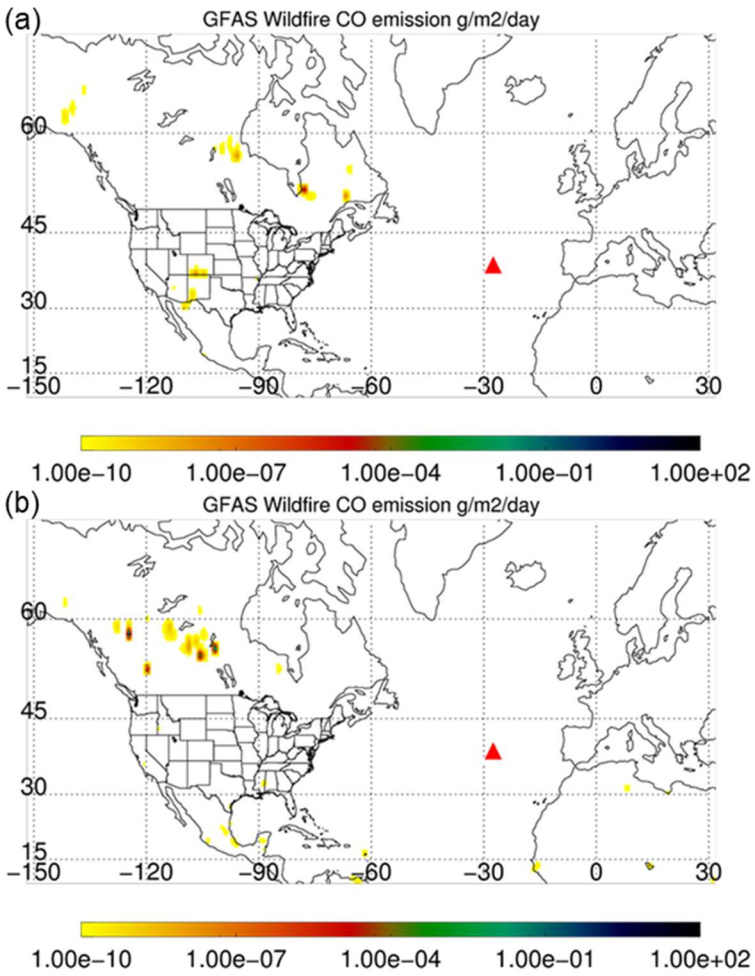

Figure S2. Wildfire emissions from GFAS dataset for the week corresponding to the PMO-1 event (a) and the PMO-3 event (b). Note the strong fire in western Quebec, which spatially corresponds to the most likely path in the PMO-1 retroplume. Multiple fires in central and western Canada may have impacted PMO-3, although they are not spatially proximate to the most likely path in the PMO-3 retroplume.

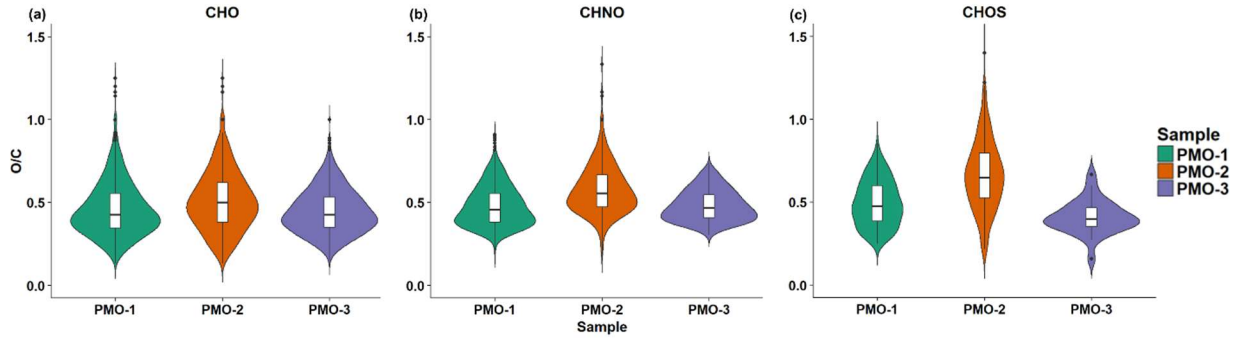

Figure S3. Violin plots showing the number distribution of species according to their O/C values separated by molecular groups.

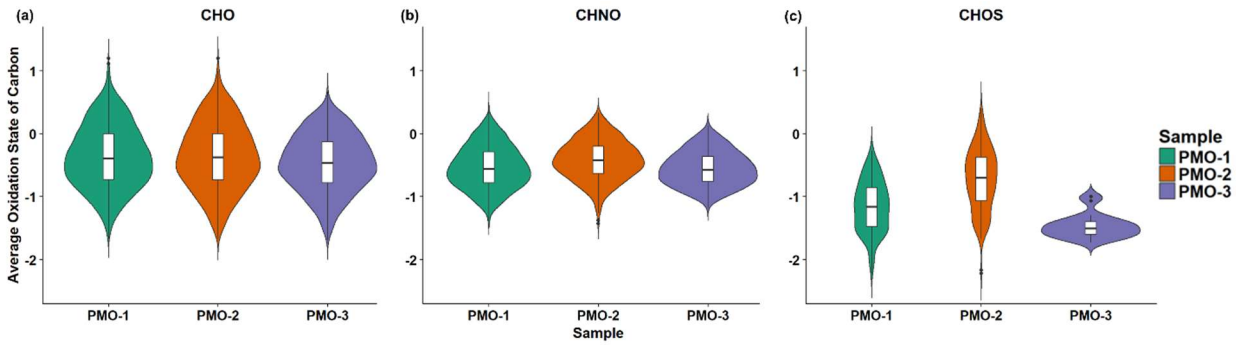

Figure S4. Violin plots showing the number distribution of species according to their OS_C values separated by molecular groups.

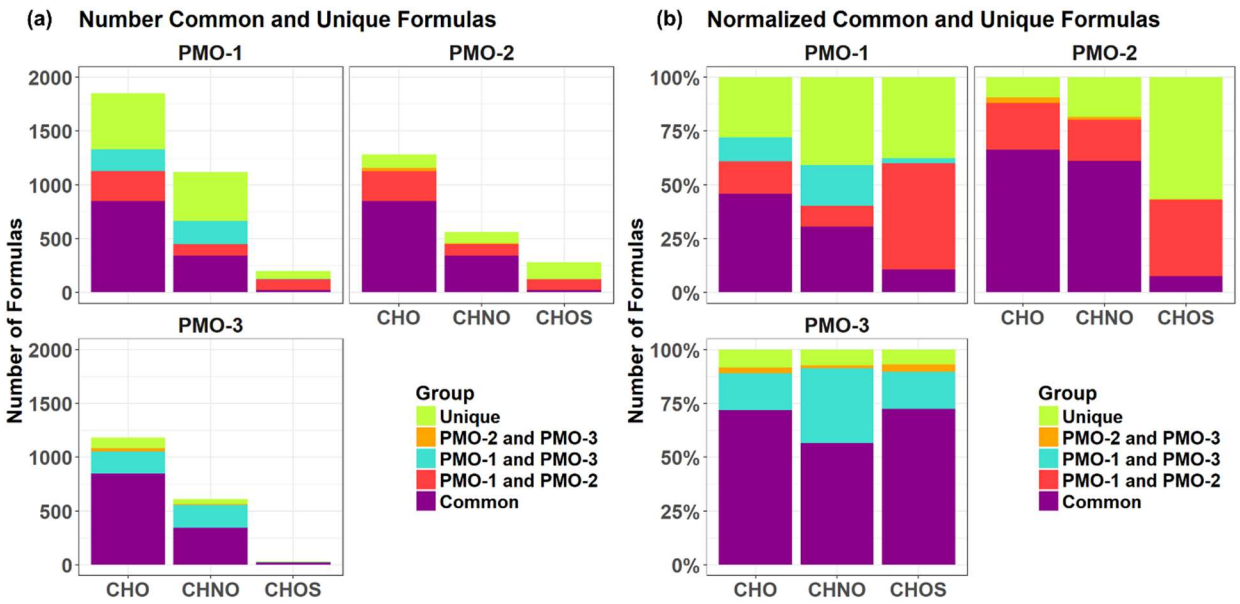

138

139 **Figure S5.** Molecular formulas common to all three samples and those unique to each sample presented as the total
140 number of formulas (a) and as a percent of total number of formulas (b).

141

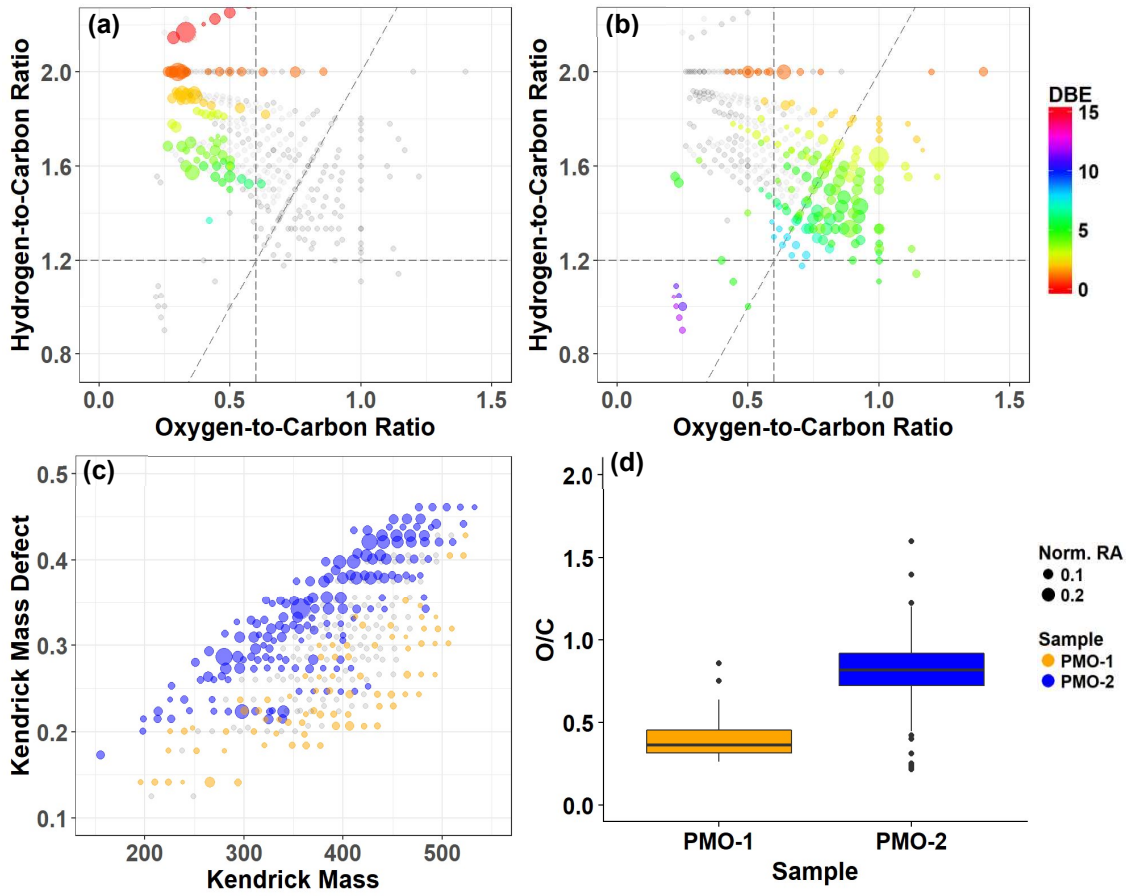

Figure S6. A comparison of PMO-1 and PMO-2 CHOS molecular formulas using van Krevelen (a, b), Kendrick plots (c), and O/C box plots (d). Common CHOS molecular formulas (grey) and unique CHOS molecular formulas (colored) are indicated in a-c.

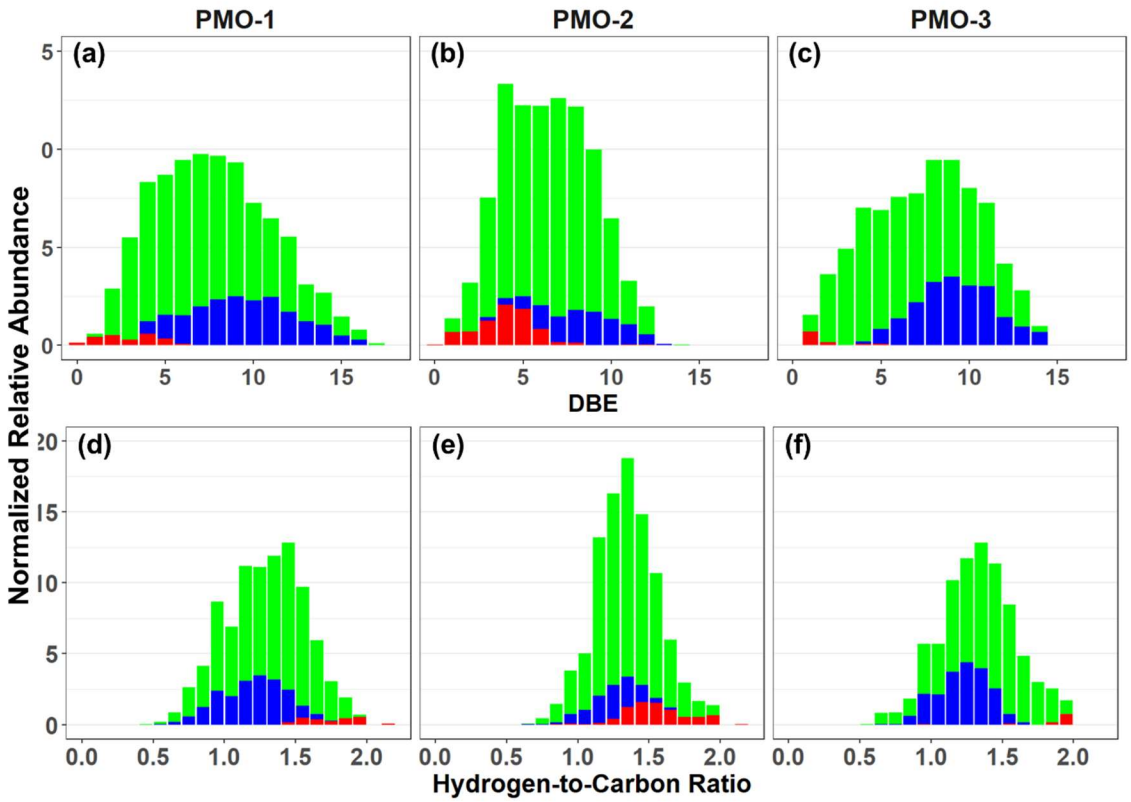

155

156 **Figure S7.** Histograms of the molecular formula DBE (a-c) and H/C (d-f).

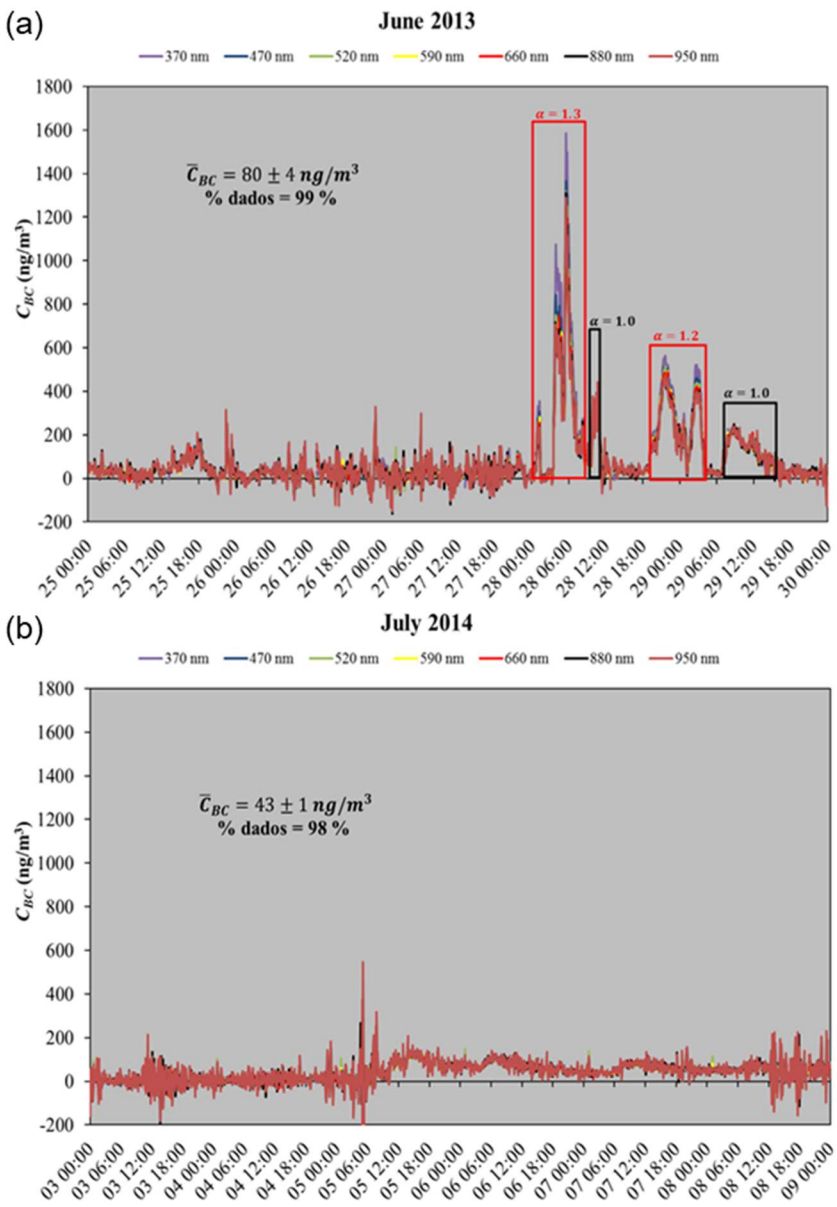

157

158 **Figure S8.** Aethalometer results for the PMO-1 (a) and PMO-2 (b) sampling periods. A few days before and after
159 each sampling period are included for reference. Note the tallest wavelength dependent peak present from
160 approximately 28 June at 00:00 to 28 June at 09:00 local time (first red box), which corresponds to the sampling period
161 of PMO-1. When the absorption angstrom exponent (α) equals 1, it suggests black carbon, when it is equal to 1.3 or
162 1.2 it suggests presence of brown carbon as well. Due to instrument maintenance/repair no data was available for the
163 time period associated with PMO-3. The sampling period for PMO-2 did not demonstrate similar peaks or wavelength
164 dependence.

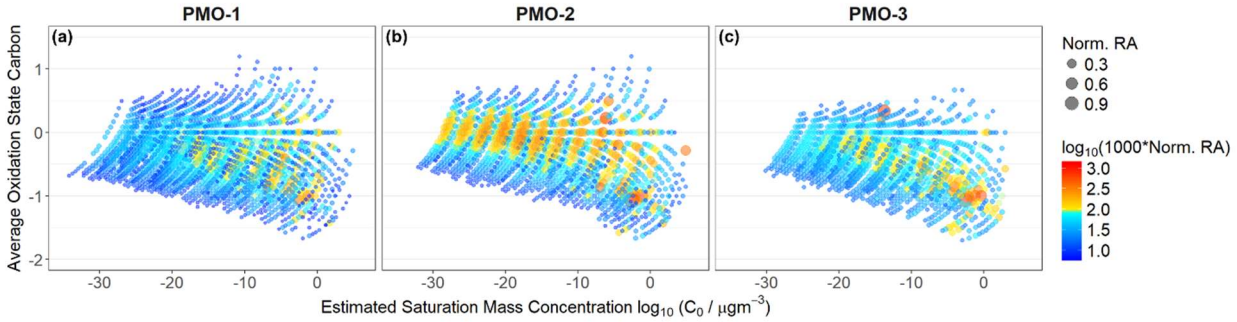

Figure S9. OS_C *vs.* volatility plots for the three samples. Volatility estimated were made using the Donahue et al. (2011) method. Only volatility for CHO species can be estimated with this method. Color is the logarithm of the normalized relative abundance multiplied by 1000. Of interest is the increased abundance of low volatility, higher oxidation species in PMO-2 relative to PMO-1 and PMO-3, indicating the importance of these species to this sample and highlighting a difference between these samples.

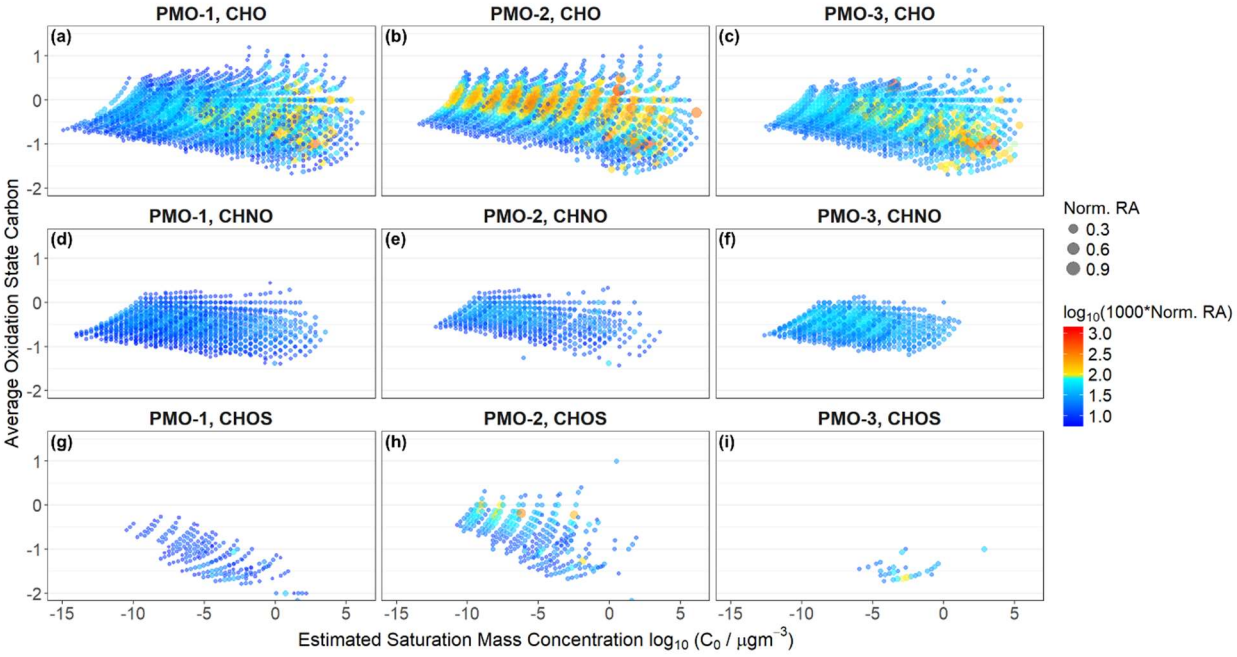

Figure S10. Group separated OS_C *vs.* volatility plots for the three samples. Volatility estimated using the Li et al. (2016) method. Color is the logarithm of the normalized RA multiplied by 1000. The same increase in abundance for low volatility, higher oxidation species is observed in this figure as in Fig. S7.

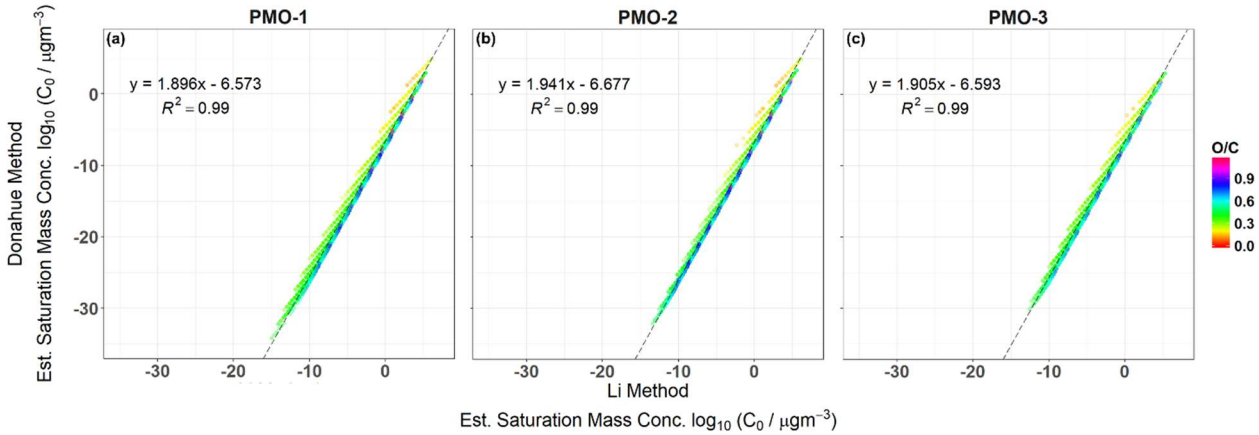

Figure S11. Correlation plot of volatility calculated by the Li et al. (2016) method and the Donahue et al. (2011) method. The comparison is linear although the slope of the line is nearly two, indicating that the Donahue method predicts values that are roughly two times what the Li method predicts, at least for the low and extremely low volatility species presented here.

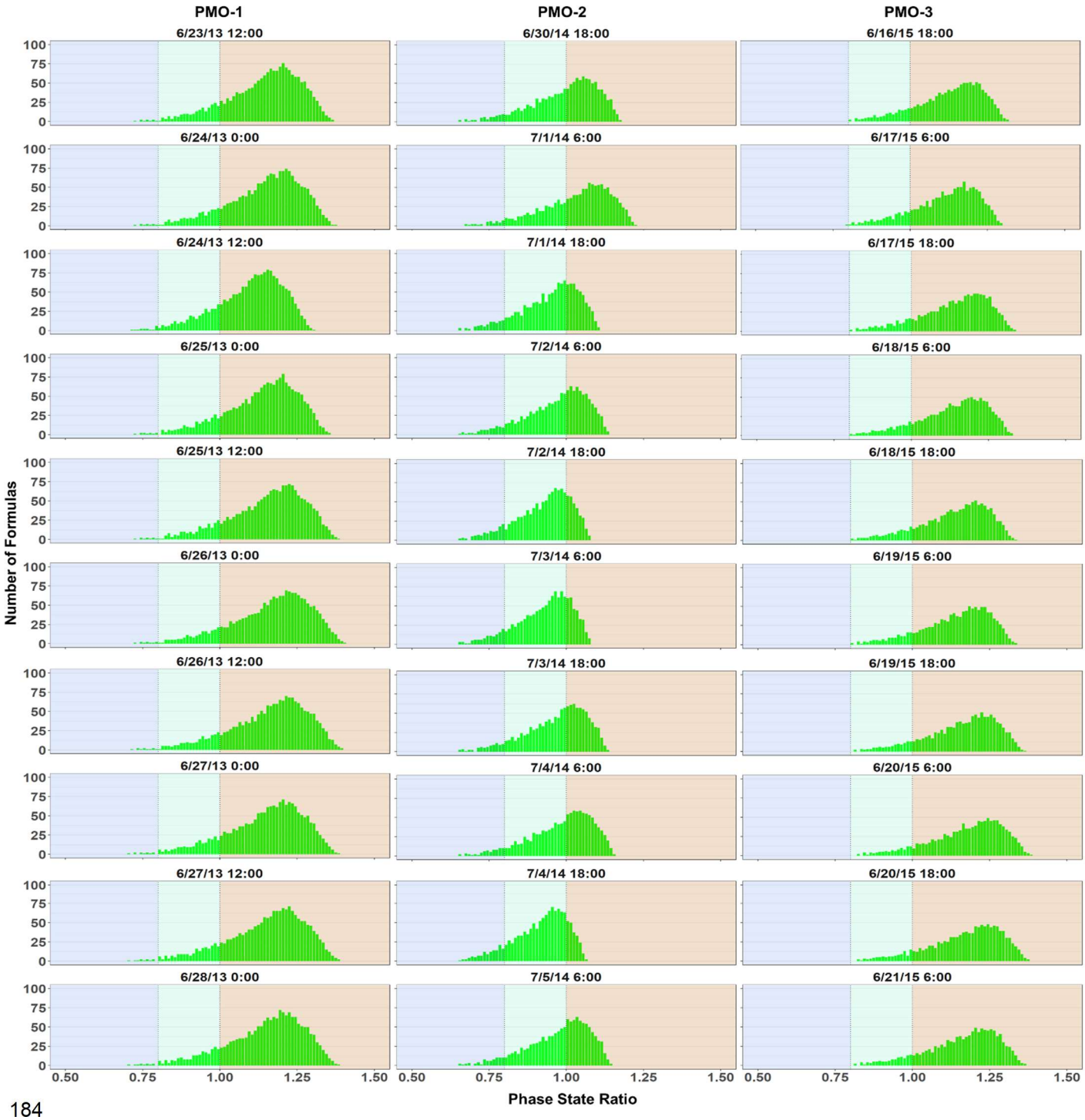

Figure S12. The distribution of phase state ratios for all of the CHO molecular formulas calculated using the 12 hour average temperature and RH values for the last 5 days. The phase state ratios corresponding to the solid, semi-solid, or liquid state are shaded with tan, green, and blue, respectively. Each column corresponds to a single sample.

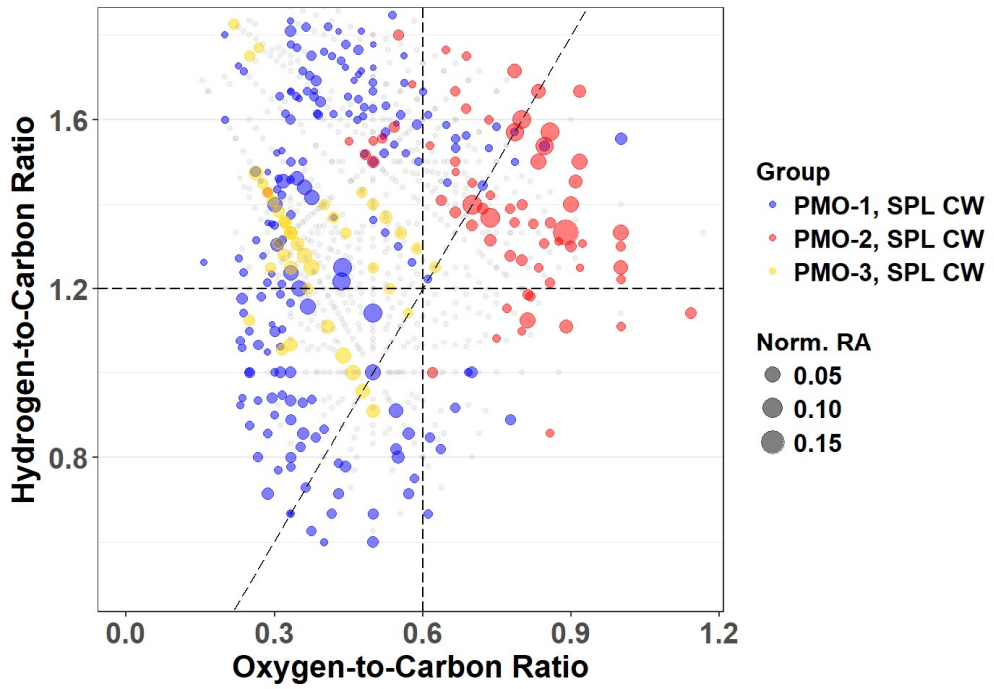

Figure S13. Van Krevelen plot showing the molecular formulas that are common to only one PMO samples and the cloud water samples from SPL. PMO-2 (red) molecular formulas located nearly exclusively in highly oxidized region of plot, may perhaps indicate cloud processing. Common molecular formulas from either PMO-1 (blue) and PMO-3 (gold) may be related to the biomass combustion that influenced the supercooled cloud water collected in the winter at SPL.

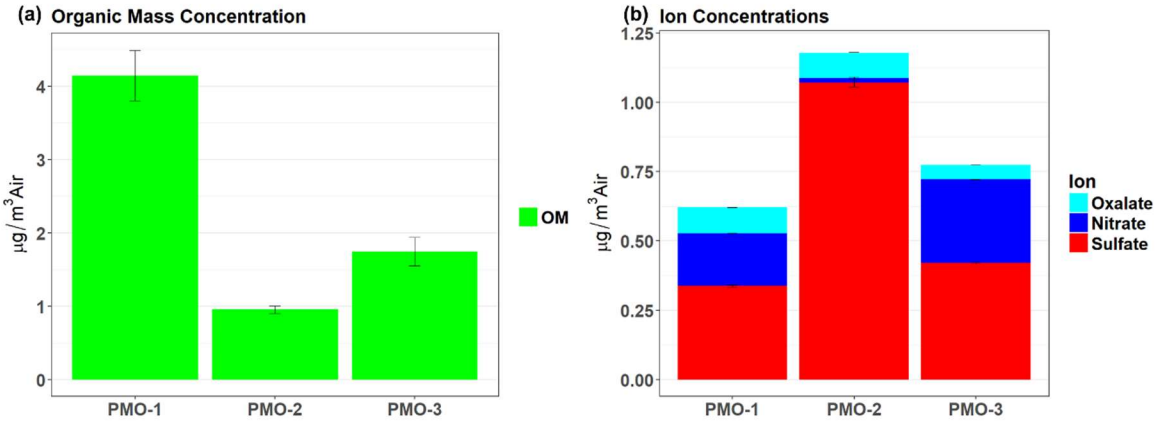

Figure S14. Organic mass concentrations (a) and sulfate, nitrate and oxalate concentrations (b).

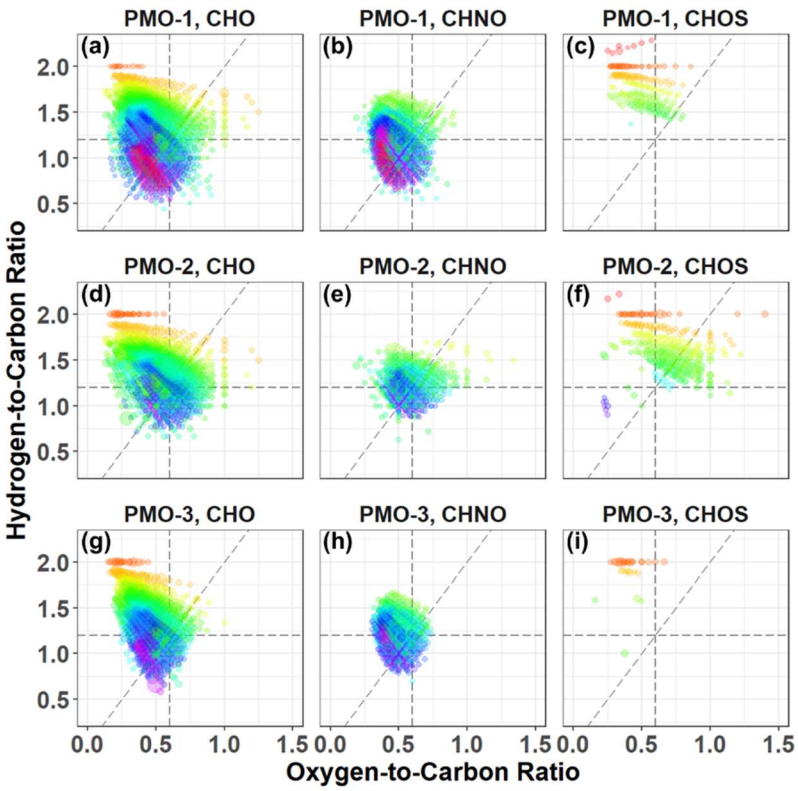

Figure S15. Group separated van Krevelen diagrams for the three samples. PMO-1 is in panels a-c, PMO-2 in panels d-f, and PMO-3 in panels g-i.

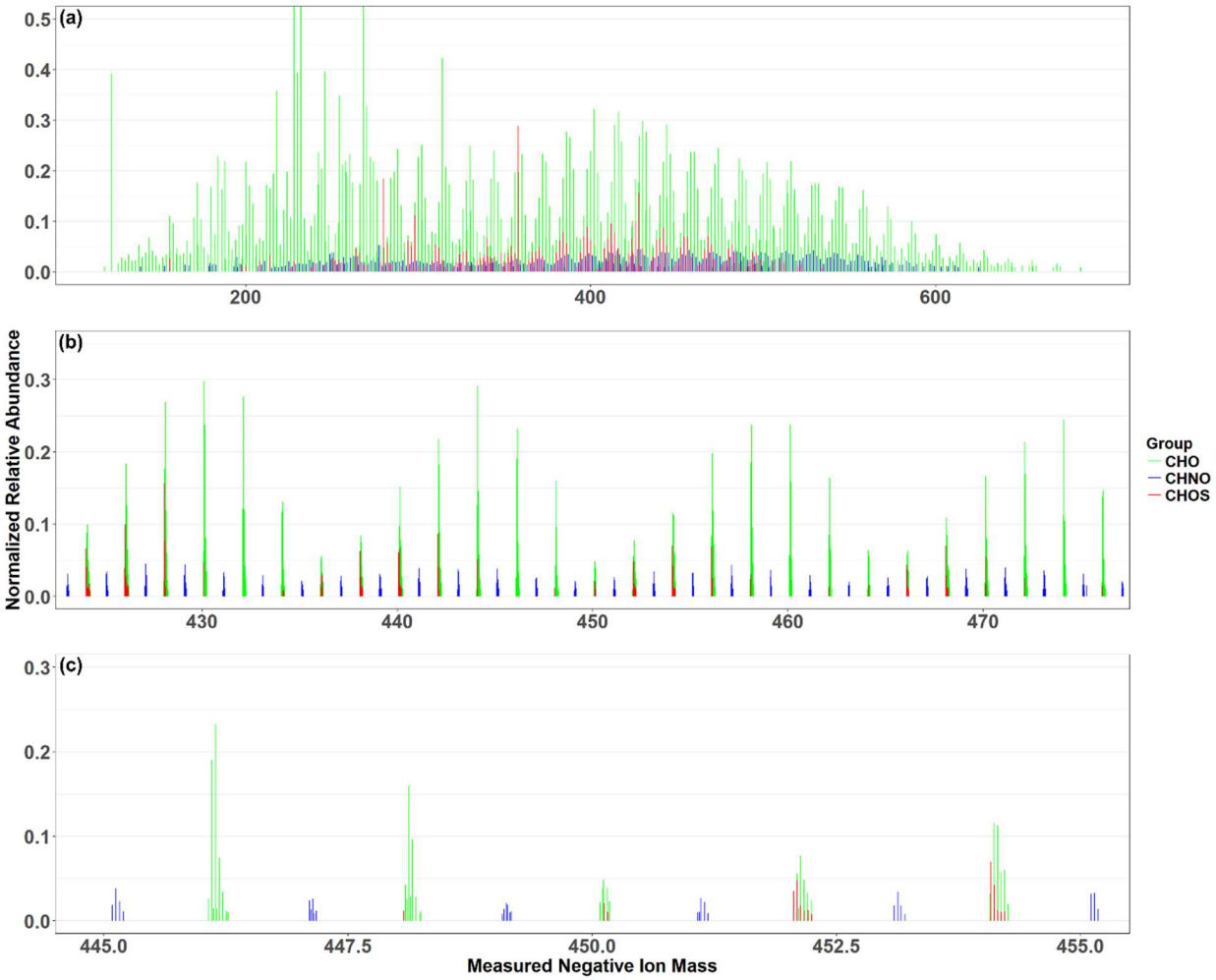

Figure S16. Progressively zoomed reconstructed mass spectrum of PMO-2 to demonstrate complexity of the sample.

Supplemental Equations

Equation S1. This is the general equation for the average oxidation state of carbon (OS_C). Sulfur and nitrogen play a role in the oxidation of the species, but it varies based on what oxidation state (Kroll et al. 2011). In this case sulfur and nitrogen are assumed to be fully oxidized.

$$OS_C \approx 2 * \frac{\#O}{\#C} - \frac{\#H}{\#C} - 5 * \frac{\#N}{\#C} - 6 * \frac{\#S}{\#C}$$

Equation S2. This is the standard equation for aromaticity index (AI) from Koch and Dittmar (2006; 2016). This is the most conservative method for calculating aromaticity as it assumes that all bonded oxygen is in carbonyl groups. The threshold for olefinic species is $0 < AI \leq 0.5$, for aromatic it is $0.5 < AI \leq 0.67$, and for condensed aromatic it is $0.67 < AI \approx 1$. All other species are defined as $AI = 0$ making them aliphatic.

$$AI = \frac{1 + C - O - S - 0.5 * H - 0.5 * N}{C - O - S - N}$$

Equation S3. Less conservative method for calculating aromaticity index from from Koch and Dittmar (2006; 2016) as it assumes that half the bonded oxygen is in carbonyl groups. The threshold for olefinic species is $0 < AI_{mod} \leq 0.5$, for aromatic it is $0.5 < AI_{mod} \leq 0.67$, and for condensed aromatic it is $0.67 < AI_{mod} \approx 1$. All other species are defined as $AI_{mod} = 0$ making them aliphatic

$$AI_{mod} = \frac{1 + C - 0.5 * O - S - 0.5 * H - 0.5 * N}{C - 0.5 * O - S - N}$$

Equation S4. Generic calculation for DBE. C represents carbon, H represents hydrogen, X represents halogens, and N represents nitrogen. Oxygen and sulfur do not play a role in the DBE calculation.

$$DBE = \#C + 1 - \frac{\#H}{2} - \frac{\#X}{2} + \frac{\#N}{2}$$

Equation S5. Glass transition temperature estimation equation from DeRieux et al., 2017. n_C^0 is the carbon reference number (12.13 ± 2.66), b_C, b_H, and b_O are the contributions of each atom to T_g, and b_{CH} and b_{CO} represent the contribution of carbon-hydrogen and carbon-oxygen bonds respectively. Values for the terms can be found in DeRieux et al. 2017. The equation determines the dry glass transition temperature, while the Gordon-Taylor Equation (Eq. S6) is required to calculate the transition temperature in non-dry conditions.

$$T_g = (n_C^0 + ln(n_C))\, b_C + ln(n_H)\, b_H + ln(n_C)\, ln(n_H)\, b_{CH} + ln(n_O)\, b_O + ln(n_C)\, ln(n_O)\, b_{CO}$$

Equation S6. Gordon-Taylor Equation as presented by DeRieux et al. (2017) to calculate the glass transition temperature in humid conditions. w_{org} is the mass fraction of organics, $T_{g,w}$ is the glass transition temperature for water (136 K), k_{GT} is the Gordan-Taylor constant (assumed to be 2.5, consistent with DeRieux et al. 2017 and Shiraiwa et al. 2017), and $T_{g,org}$ is the dry glass transition temperature calculated by Eq. S5. For greater detail see DeRieux et al. 2017 and Shiraiwa et al. 2017.

$$T_g(w_{org}) = \frac{(1 - w_{org})T_{g,w} + \frac{1}{k_{GT}} w_{org} T_{g,org}}{(1 - w_{org}) + \frac{1}{k_{GT}} w_{org}}$$

Equation S7. Adapted Gordon-Taylor equation for use with inputs for relative humidity (RH), dry glass transition temperature, and ambient temperature. This generates the phase state ratio (PSR), which predicts the phase the molecular species is likely in, PSR >= 1 is solid, PSR >= 0.8 & PSR < 1 is semi-solid, and PSR < 0.8 is liquid. This equation converts w_{org} to a relative humidity dependent term as described in DeRieux et al. (2017) and Shiraiwa et al. (2017), and converts $1/k_{GT}$ to 0.4, which is its value using the assumption of k_{GT} equals 2.5. T_{amb} is the ambient temperature.

$$\text{Phase State Ratio} = \frac{\left(\frac{\left(1 - \frac{1.4 - \frac{1.4 * RH}{100}}{1.4 - \frac{1.28 * RH}{100}}\right) * 136 + 0.4 * \left(\frac{1.4 - \frac{1.4 * RH}{100}}{1.4 - \frac{1.28 * RH}{100}}\right) * T_{g,org}}{\left(1 - \frac{1.4 - \frac{1.4 * RH}{100}}{1.4 - \frac{1.28 * RH}{100}}\right) + 0.4 * \left(\frac{1.4 - \frac{1.4 * RH}{100}}{1.4 - \frac{1.28 * RH}{100}}\right)} \right)}{T_{amb}}$$

References

Chang, O., Procedure for the analysis of particulate anions and cations in motor vehicle exhaust by ion chromatography, California EPA Air Resources Board, 2011

DeRieux, W. W., Li, Y., Lin, P., Laskin, J., Laskin, A., Bertram, A. K., Nizkorodov, S. A. and Shiraiwa, M.: Predicting the glass transition temperature and viscosity of secondary organic material using molecular composition, Atmos. Chem. Phys. Disc., 1–41, doi:10.5194/acp-2017-1066, 2017.

Donahue, N., Epstein, S., Pandis, S. and Robinson, A.: A two-dimensional volatility basis set: 1. organic-aerosol mixing thermodynamics, Atmos. Chem. Phys., 11(7), 3303–3318, doi:10.5194/acp-11-3303-2011, 2011.

Dzepina, K., Mazzoleni, C., Fialho, P., China, S., Zhang, B., Owen, R. C., Helmig, D., Hueber, J., Kumar, S., Perlinger, J. A., Kramer, L. J., Dziobak, M. P., Ampadu, M. T., Olsen, S., Wuebbles, D. J., and Mazzoleni, L. R.: Molecular characterization of free tropospheric aerosol collected at the Pico Mountain Observatory: a case study with a long-range transported biomass burning plume, Atmos. Chem. Phys., 15(9), 5047–5068, doi:10.5194/acp-15-5047-2015, 2015.

Honrath, R. E., Helmig, D., Owen, R. C., Parrish, D. D. and Tanner, D. M.: Nonmethane hydrocarbons at Pico Mountain, Azores: 2. Event-specific analyses of the impacts of mixing and photochemistry on hydrocarbon

ratios, Journal of Geophysical Research: Atmospheres (1984–2012), 113(D20), doi:10.1029/2008jd009832, 2008.
Kleissl, J., Honrath, R. E., Dziobak, M. P., Tanner, D., Val Martín, M., Owen, R. C. and Helmig, D.: Occurrence of upslope flows at the Pico mountaintop observatory: A case study of orographic flows on a small, volcanic island, J. Geophys. Res-Atmos., 112(D10), doi:10.1029/2006jd007565, 2007.
Koch, B. P. and Dittmar, T.: From mass to structure: an aromaticity index for high-resolution mass data of natural organic matter, Rapid Commun. Mass Sp., 20(5), 926–932, doi:10.1002/rcm.2386, 2006.Koch, B. P. and Dittmar, T.: From mass to structure: an aromaticity index for high-resolution mass data of natural organic matter, Rapid Commun. Mass Sp., 30(1), 250, doi: 10.1002/rcm.7433, 2016.

Kroll, J. H., Donahue, N. M., Jimenez, J. L., Kessler, S. H., Canagaratna, M. R., Wilson, K. R., Altieri, K. E., Mazzoleni, L. R., Wozniak, A. S., Bluhm, H., Mysak, E. R., Smith, J. D., Kolb, C. E. and Worsnop, D. R.: Carbon oxidation state as a metric for describing the chemistry of atmospheric organic aerosol, Nat. Chem., 3(2), nchem.948, doi:10.1038/nchem.948, 2011.

Li, Y., Pöschl, U. and Shiraiwa, M.: Molecular corridors and parameterizations of volatility in the chemical evolution of organic aerosols, Atmos. Chem. Phys., 16(5), 3327–3344, doi:10.5194/acp-16-3327-2016, 2016.
Mazzoleni, L. R., Saranjampour, P., Dalbec, M. M., Samburova, V., Hallar, A. G., Zielinska, B., Lowenthal, D. H. and Kohl, S.: Identification of water-soluble organic carbon in non-urban aerosols using ultrahigh-resolution FT-ICR mass spectrometry: organic anions, Environ. Chem., 9(3), 285–297, doi:10.1071/en11167, 2012.
Olivier, J.G.J. and Berdowski, J.J.M.: Global emissions sources and sinks, in: The Climate System, Berdowski, J., Guicherit, R. and Heij, B.J., A.A. Balkema Publishers/Swets & Zeitlinger Publishers, Lisse, The Netherlands. 33-78, 2001.
Owen, R. C. and Honrath, R. E.: Technical note: a new method for the Lagrangian tracking of pollution plumes from source to receptor using gridded model output, Atmospheric Chemistry and Physics, 9(7), 2577–2595, doi:10.5194/acp-9-2577-2009, 2009.
Rémillard, J., Kollias, P., Luke, E. and Wood, R.: Marine Boundary Layer Cloud Observations in the Azores, J. Climate, 25(21), 7381–7398, doi:10.1175/jcli-d-11-00610.1, 2012.
Seibert, P. and Frank, A.: Source-receptor matrix calculation with a Lagrangian particle dispersion model in backward mode, Atmospheric Chemistry and Physics, 4(1), 51–63, doi:10.5194/acp-4-51-2004, 2004.
Shiraiwa, M., Li, Y., Tsimpidi, A., Karydis, V., Berkemeier, T., Pandis, S., Lelieveld, J., Koop, T. and Pöschl, U.: Global distribution of particle phase state in atmospheric secondary organic aerosols, Nat. Commun., 8, ncomms15002, doi:10.1038/ncomms15002, 2017.
Stohl, A., Forster, C., Frank, A., Seibert, P. and Wotawa, G.: Technical note: The Lagrangian particle dispersion model FLEXPART version 6.2, Atmospheric Chemistry and Physics, 5(9), 2461–2474, doi:10.5194/acp-5-2461-2005, 2005.
Zhang, B., Owen, R. C., Perlinger, J. A., Helmig, D., Val Martín, M., Kramer, L., Mazzoleni, L. R. and Mazzoleni, C.: Ten-year chemical signatures associated with long-range transport observed in the free troposphere over the central North Atlantic, Elem. Sci. Anth., 5, doi:10.1525/elementa.194, 2017.